RSC Advances

ROYAL SOCIETY OF CHEMISTRY

www.rsc.org/advances

p-aminobenzoic acid (pABA) sensitization of LaF_3:Tb^{3+} nanoparticles and its applications in detection of explosive materials

Debasish Ghosh and Meitram Niraj Luwang*

Chemical Engineering and Process Development Division

National Chemical Laboratory, Pune - 411008 (INDIA)

ABSTRACT

This work reports the utilization of water dispersible terbium (Tb^{3+}) doped spherical LaF_3 nanoparticles (~5 nm) surface functionalised with *p*-aminobenzoic acid (pABA) for the detection of aromatic nitro explosives. The functionalised nanoparticles show remarkable sensitivity to a number of highly electron deficient aromatic nitro compounds like picric acid (PA), 2,4,6-trinitrotoluene (TNT), 2,4-dinitrotoluene (2,4-DNT), 2,4-dinitrophenol (2,4-DNP) etc. All of these nitro compounds can be detected easily at ppm level using this luminescence quenching technique whereas in case of TNT it detects as low as 50 ppb concentration level. This novel approach of utilising the Tb^{3+} doped NPs sensitised by pABA have potential application in the detection of explosive materials.

Keywords: Nanomaterials, Lanthanide, Explosives, Photoluminescence. Quenching

Corresponding author

mn.luwang@ncl.res.in (Meitram Niraj Luwang)

Ph: (+91) 20 2590 2950

Fax: (+91) 20 2590 2621

1. INTRODUCTION

An explosive material is generally a reactive substance which has a great amount of potential energy that can give an explosion accompanied by light, heat, sound and pressure. Among the explosive materials, nitro compounds like picric acid, 2,4-dinitrotoluene (2,4-DNT), 2,4,6-trinitrotoluene (TNT), 1,3,5-trinitroperhydro-1,3,5-triazine (RDX), etc. are some of the generally used components.[1-6] Apart from being used as an explosive material, nitro compounds like TNT are hazardous to human health which can cause various health concern like anaemia, abnormal liver function, etc.[7,8] Considering the hazardous nature of the nitro compounds in terms of both security concerns and as a pollutant, the need for the detection of these materials has been the primary importance.

Researchers all over the globe have been working on various techniques for the detection of explosive material. Some of the known techniques are metal detectors which generally detect metal based weapons, dogs with their superior sensing capabilities, X-ray machines by analysing the density of the materials, neutron activation where the explosive materials is bombarded with neutrons which gives its elemental composition, and so on.[9-12] Apart from the above mention techniques, spectroscopic techniques especially fluorescence based chemosensors, due to their high sensitivity and probability of using as a hand held devices for in-field detection have superior advantage.[13,14] Generally, in this approach, the fluorescent materials on interaction with the explosives materials either turn-off or quenches the luminescent of the sensors, which relies on an oxidative quenching mechanism.[14] In detail, the sensor material plays the role of an electron donor and aromatic nitro compounds as an electron acceptor due to the presence of their electron withdrawing nitro groups. On excitation with photon, an electron is transferred from the sensor materials to the analyte, leading to oxidation of the excited state, thereby quenching the fluorescence of the sensors. Some of the generally used fluorescent materials are conjugated polymers,[15] metal complexes,[16] dendrimers,[17] carbon nanotubes,[18] and recently the use of metal-organic framework (MOF)[19,20] as the new generation of sensors materials for explosive detection.
Because of the unique characteristics of lanthanide luminescence (sharp emission, emission in whole spectral range, long lived emission, etc.) lanthanides have attracted special attention due to their wide variety of applications.[21-24]

The lanthanide complexes have been widely investigated over the past three decades due to their enhanced luminescence properties. In the lanthanide complexes, the co-ordinated organic molecule is first excited with proper wavelength and then the excited molecule

effectively transfers its energy to the lanthanide ion and produces enhanced luminescence.[25,26] But the complexes have some limitations like quenching of the excited state of the lanthanide ion by the vibrational overtones of -OH, -NH, and -CH groups present in the organic molecule or in the medium.

Generally, in lanthanide doped materials, the lanthanide ions act as a guest in certain host materials. The host just not only provides matrix to the lanthanide ion but also protects the lanthanide ion from being quenched by the environmental quenchers like $–NH_2$, H_2O etc.[27] The host material is first excited with proper wavelength and then the excited molecule effectively transfers its energy to the lanthanide ion thereby resulting in a sensitised luminescence.[28] But most of the commonly used host materials viz YPO_4, YVO_4, CeO_2 etc. have very high phonon energies which quench the excited states of the lanthanide ions in non-radiative way and therefore reduce the radiative luminescence.[28-30] LaF_3 is well established as a good host material due to its very low phonon energies (<400 cm^{-1}), high solubility of lanthanide ions in its matrix and thermal stability.[31] But, as LaF_3 is an insulator its high band gap does not allow it to absorb UV light hence light cannot be generated by exciting the nanoparticles in the host absorption region.[32] To overcome this limitation, the lanthanide ions on the surface of the nanoparticles are allowed to form complex with organic molecules that can absorb UV or IR light and effectively transfers it to the lanthanide ion.[27,33,34] Recently, lanthanide doped nanoparticles have been utilised for the selective detection of explosive materials via inkjet printing and magnetic separation.[35,36]

In this work, we report that *p*-aminobenzoic acid (pABA) sensitised Tb^{3+} ion doped LaF_3 nanoparticles has been used for the detection of nitro compounds. Herein, the pABA sensitised the photoluminescence properties of Tb^{3+} which on interaction with the selected nitro compound quenches the enhanced photoluminescence properties. The properties of the nanomaterials has been analysed by various characterisation techniques and at varying concentration of the luminescent centre, analytes and at different pH.

2. EXPERIMENTAL SECTION

2.1 Reagents and Materials

Lanthanum nitrate hexahydrate ($La(NO_3)_3.6H_2O$) (99.99%), terbium nitrate pentahydrate ($Tb(NO_3)_3.5H_2O$) (99.9%), Ammonium fluoride (NH_4F) (99.99%) were purchased from Aldrich. Anhydrous citric acid (99.5%) and dimethyl sulfoxide (99.9%) were purchased from Merck. *p*-aminobenzoic acid from SDFCL and picric acid (PA) obtained from Aldrich. All

the others nitro compounds listed below are obtained from DRDO-HERML, Pune. The abbreviated term (parenthesis) for nitro compounds are as follows; nitrobenzene (NB), o-nitrophenol (2-NP), o-nitrotoluene (2-NT), 2,4-dinitrotoluene (2,4-DNT), 2,6-dinitrotoluene (2,6-DNT), 2,4-dinitrophenol (2,4-DNP), picric acid (PA), 2,4,6-trinitrotoluene (TNT) and some aliphatic nitro compounds such as nitromethane (NM), 1,2,4-butanetriol nitrate (BTTN), octahydro-1,3,5,7-tetranitro-1,3,5,7-tetrazocine (HMX), and 1,3,3-Trinitroazetidine (TNAZ). Deionised water was used to make aqueous solutions. All the materials were used as received.

2.2 Synthesis of $LaF_3:Tb^{3+}$ spheres

$Tb_xLa_{1-x}F_3$ (where x = 0.02, 0.04, 0.06, 0.08 and 0.1) nanoparticles were synthesised following some previously reported works with minor modifications.[37,38] 3g of anhydrous citric was dissolved in 20 ml of water in 250 ml round bottom flask. 60 ml of DMSO and 1 ml conc. NH_4OH were added to the citric acid solution to adjust the pH to 5-6 and stirred nicely. About 2 mmol (depending upon doping conc.) of lanthanum nitrate hexahydrate ($La(NO_3)_3.6H_2O$) and stoichiometric amount of terbium nitrate pentahydrate ($Tb(NO_3)_3.5H_2O$) were dissolved in 2 ml water. This lanthanide solution was added drop wise to the citric acid solution at 70 °C temperature. A dense white turbidity appeared. White dense turbidity converted to a pale white suspension when 3ml aq. solution of 7 mmol NH_4F was added slowly. The reaction mixture was refluxed at 110 °C temperature under water circulation for two hours and then cooled to room temperature. The nanoparticles were collected by centrifugation, washed with deionised water and methanol, and dried at room temperature.

2.3 Surface-functionalization of nanoparticles

0.2 g of the resulting nanoparticles was dispersed in 50 ml water and formed a colloidal solution. 0.2 g of *p*-aminobenzoic acid was dissolved in 30 ml NaOH solution. This *p*-aminobenzoic acid solution was added slowly to the nanoparticles colloid at 65 °C and refluxed for two hours at 75 °C. The surface-functionalised nanoparticles were separated by centrifugation, washed twice with water and methanol and dried at room temperature.

2.4 Preparation of nanoparticle dispersion

100 mg of the $LaF_3:Tb^{3+}$(8%)@pABA was nicely dispersed in 250 ml of 2×10^{-3} (M) HCl solution by sonication and this dispersion was used for sensitization experiment and all the analyte concentration measurements.

2.5 Preparation of analyte solution

500 mg picric acid was dissolved in 1000 ml water to prepare a stock solution of 500 ppm (2.18 mM) strength. This mother solution was followed by a two-fold serial dilution to prepare the solutions of 250, 125, 62.5, 31, 15.5, 8, 4, 2 ppm concentrations. These analyte solutions were mixed with equal volume of the dispersion of the nanoparticles and analysed, i.e, the analyte concentrations in the experimental solutions were again diluted to half concentration and pH of the resulting solution were maintained at pH = 3.

3 mg of TNT was dissolved in 25 ml water to prepare a 120 ppm (0.52 mM) stock solution. This solution was diluted with water to prepare 100 ppm, 80 ppm, 60 ppm, 40 ppm, 20 ppm solutions which on mixing with equal volume dispersion of nanoparticles gave the experimental solutions. A 2000 ppb solution of TNT was diluted with water to prepare 1600 ppb, 800 ppb, 400 ppb, 100 ppb solutions which were used for the experiments.

7 mg of nitrophenol was dissolved in 250 ml of water to prepare a 0.2 mM stock solution (28 ppm). This solution was diluted with water to prepare 14 ppm, 7 ppm and 3.5 ppm solution which on mixing with equal volume of nanoparticles dispersion gave the desired experimental solutions (14 ppm, 7 ppm, 3.5 ppm and 1.75 ppm). As for 2,4-dinitrophenol and 2,4-dinitrotoluene, 9 mg each of the analyte was dissolved in 250 ml of water to prepare a 0.2 mM stock solution (36 ppm). This solution was diluted with water to prepare 18 ppm, 9 ppm and 4.5 ppm solution which on mixing with equal volume dispersion of nanoparticles gave the desired experimental solutions (18 ppm, 9 ppm, 4.5 ppm and 2.25 ppm).

For the preparations of 0.2 mM solutions the remaining analyte under study, 6.9, 7, 6, 9, 3, 9, 12, 9.6, 11 and 15 mg of 2-NT, 2-NP, NB, 2,4-DNP, NM, 2,4-DNT, BTTN, TNAZ, RDX and HMX, respectively were dissolved in 250 ml of water , which on mixing with equal volume dispersion of nanoparticles gave the desired experimental solutions (0.1 mM).

2.6 Characterisation

The X-ray diffraction (XRD) of powder samples was examined on a Xpert-Philips diffractometer using Cu Kα radiation (λ = 0.15405 nm) powder X-ray diffraction

(PANalytical X'Pert Pro dual goniometer diffractometer) with filtered Cu Kα at 40 kV and 30 mA and X'celerator solid state detector. The diffraction pattern is obtained at room temperature in Bragg-Brentano geometry. Powder samples were mounted on a sample holder and scanned in the range 2θ = 5 to 90.

The functional characteristics of the nanoparticles were recorded using Fourier Transform Infrared Spectrometer (Perkin-Elmer, Q-50000 GX Spectrometer). The recording of spectrum was done in the wavelength range from 4000 to 400 cm^{-1}. Powder samples were studied by making thin pellets with KBr. All the UV-visible measurements are done in Shimadzu UV-1601 PC UV Visible double beam spectrophotometer.

All the luminescence spectra and decay lifetimes were recorded at room temperature for the samples in aqueous medium using an EDINBURGH instrument FLS920 equipped with 450 W Xenon lamp having Peltier element cooled red sensitive Hamamatsu R955 PMT and a 100W microsecond flash lamp.

High resolution transmission electron microscopy (HRTEM) studies of the nanoparticles were done on A FEITECNAI 3010 electron microscope operating at 300 kV (Cs = 0.6 mm, resolution 1.7 Å). Samples were crushed and dispersed in isopropanol before depositing onto a holey carbon grid. Energy dispersive X-ray (EDX) measurements were performed on a scanning electron microscope (SEM) system (FEI, Model Quanta 200 3D) equipped with an EDX attachment. Dynamic Light Scattering (DLS) measurements were performed on Melvern (U. K.) instrument ZS90 Nanoseries model with zeta size of 0.2 nm to 6 micron. The samples were dispersed in isopropanol and sonicated for 30 minute before the measurement.

3. RESULTS AND DISCUSSION

3.1 XRD study

The XRD analysis of $LaF_3:Tb^{3+}$ and $LaF_3:Tb^{3+}$@PABA samples for various concentrations of Tb^{3+} were performed in order to investigate the crystal structure, effect of doping and surface functionalization on the prepared nanomaterials. All the samples (before and after surface functionalization) had clear resemblance with the tysonite structure of LaF_3 (JCPDS 82-0690) as shown in Figure 1a-c. No extra peaks corresponding to the impurity phase were observed indicating the formation of the clear LaF_3 phase and successful doping of the lanthanide ions (Tb^{3+}). The peaks are generally board in nature which indicate that the prepared nanomaterials are in small size range. The average crystallite size of the

nanoparticles were calculated using Scherrer equation ($d = k\lambda/\beta\cos\theta$), where λ is the X-ray wavelength (0.154 nm), β is the full width at half-maximum (fwhm) of a diffraction peak, θ is the diffraction angle, k is a constant (0.89). Average crystallite size of $LaF_3:Tb^{3+}$ and $LaF_3:Tb^{3+}$@pABA nanoparticles are in the range of (5.52 - 6.29) and (4.50 - 5.53) nm respectively, at different concentration of the dopant, Tb^{3+} as summarised in Table 1. There is a broadening of peaks after the surface functionalization as can be observed from the gradual increase in the FWHM value of the (111) plane from (2.49 – 2.71) to (2.70 – 3.12) nm as we move from $LaF_3:Tb^{3+}$ to $LaF_3:Tb^{3+}$@PABA nanoparticles (Table 1). There is a slight reduction in the unit cell volume of the compound with the increase of the dopant concentration (Tb^{3+} ions). The reason for the shrinking phenomenon of the unit cell volume is due to the smaller ionic radius of Tb^{3+} (0.923 Å) as compared to that of La^{3+} ion (1.032 Å).[39] The above observation further confirms the successful substitution of Tb^{3+} ions in the crystalline LaF_3 lattices. All the above analysis indicates that Tb^{3+} ions have been successfully doped into the lattice of LaF_3 nanomaterials.

3.2 IR study

Figure 1d-e shows the FTIR spectra of $LaF_3:Tb^{3+}$ and $LaF_3:Tb^{3+}$@pABA nanoparticles in order to analyse the substitution of citric acid by pABA on the nanoparticles surface. The broad peak (Figure 1d) in the range of 3000 - 3500 cm^{-1} can be assigned to the stretching vibration of O-H group of carboxylic acid. Peaks at 1583 cm^{-1} and 1410 cm^{-1} are assigned to asymmetric and symmetric stretching vibrations of carboxylic group.[34] Strong peak at 1016 cm^{-1} is due to C-O stretching of citric acid.[40] The spectra of the functionalised nanoparticles (Figure 1e) show two new peaks at 1497 $cm^{-1}$and 747 cm^{-1} which are due to C-C stretching vibration and out of plane C-H bending vibrations of benzene ring, respectively.[33,41] The peaks at 1558 cm^{-1} and 1400 cm^{-1} are due to the carboxylic acid group of pABA. Broad peak above 3000 cm^{-1} can be assigned to amine group of pABA. From the above analysis, we confirmed that pABA has been successfully attached on the surface of the nanoparticles.

3.3 Morphology and elemental composition analysis

In this work, we observed important morphological change of the nanoparticles synthesised under similar experimental conditions, depending upon the doping concentrations of the Tb^{3+} ion. Figure 2a-c show the HRTEM images of as prepared surface functionalised

LaF_3:Tb^{3+}@pABA NPs which show the morphology of spherical shape. The average size of the spherical nanoparticles is 5.2 nm which is in good agreement with the value calculated from XRD. The lattice fringes are clearly observed and the experimentally observed d-spacing is found to be 0.32 nm which coincides with the (111) plane of tysonite structure (JCPDS 82-0690) of LaF_3. Crystalline nature of the nanoparticles is well understood from the SAED pattern (Figure 2d) and the major diffraction has been assigned to their corresponding planes. Figure 2e shows the EDX spectra of as-prepared LaF_3:Tb^{3+}@pABA NPs. All the typical peaks corresponding to La, F, Tb are observed in the spectra. At higher dopant concentration (10 at% of Tb^{3+}), the spherical shape morphology of the nanoparticles get converted to a rod shape morphology as shown in Figure 2f. The rods have average length ~10 nm and width ~2 nm.

The particles are found to be agglomerated in nature. Figure S1 (see ESI) shows the histogram of particle size distribution from the DLS measurement. The individual particles are found to be agglomerated in the size range of ~120-170 nm with ~150 nm constituting half of the total populations.

3.4 Absorption study

The absorption spectra of pABA functionalised and non-functionalised LaF_3:Tb^{3+} nanoparticles are shown in Figure 3a. In case of functionalised nanoparticles a new strong broad absorption peak having maximum at 265 nm appears which is not present for as prepared non-functionalised LaF_3:Tb^{3+} nanoparticles. The peak can be assigned to the absorption peak of pABA which is due to the presence of $–NH_2$ group where it is in conjugation with the benzene ring.[42] UV absorption property of pABA is highly sensitive to the pH of the medium. Many authors reported that the conversion of $–NH_2$ to $–NH_3^+$ in strongly acidic medium is accompanied by marked reduction in absorption.[43,44] Due to protonation, lone pair of electron on nitrogen atom of $–NH_2$ group is no more available for conjugation with aromatic ring leading to the decrease in the absorption intensity. The functionalised nanoparticles show lowest absorption intensity at pH = 1 (Figure S2, See ESI). Surprisingly, absorption intensity is highest at pH = 3 which is almost double as compared to the absorption intensity at pH = 7. The reason might be the occurrence of the $–NH_2$ form of pABA at pH = 3. Krishna *et al.*[45] have reported that pABA exists dominantly in three different acid-base states ranging from the fully protonated ($-NH_3^+$; pH = 1), through neutral ($-NH_2$; pH = 3.3), to anionic ($-COO^-$; pH = 10), and its subsequent change from electron-

acceptors to electron-donors with increasing pH. The above analysis further confirms that the pABA sensitised $LaF_3:Tb^{3+}$ shows highest absorption activity at pH = 3 and subsequently all the photoluminescence analysis have been performed at this optimum pH. Very low UV absorption in the alkaline medium where free $-NH_2$ group is present is due to very little dispersibility of the nanoparticles at pH = 13.

3.5 Photoluminescence studies

All the photoluminescence studies were performed in aqueous medium. 50 mg/250 ml aqueous (pH = 3) dispersions of pABA functionalised and non-functionalised $LaF_3:Tb^{3+}$ samples were taken to examine the energy transfer or sensitization of Tb^{3+} by pABA. Figure 3b shows the excitation spectra of pABA functionalised and non-functionalised $LaF_3:Tb^{3+}$ nanoparticles at the fixed emission wavelength of 546 nm. When the functionalised nanoparticles are excited at pABA absorption maximum at 265 nm, it gives ~100 times stronger luminescence as compared to direct excitation (360 nm) of Tb^{3+} ion as shown in Figure 3c. This indicates that there is a successful transfer of energy from pABA molecules to Tb^{3+} ions and pABA acts as an effective sensitizer for Tb^{3+} ions. In case of direct excitation of Tb^{3+} by 360 nm effective excited state is not generated due to forbidden nature of f-f transition. But in case of sensitization effective energy transfer takes place between Tb^{3+} and pABA when excited at 265 nm. In this case Tb^{3+} has a highly populated excited state. Thus radiative transition from the excited state to ground state gives 100 times enhanced luminescence.

The energy transfer process can be explained through the schematic diagram, Figure 3d. Here, when a photon (*hv*) of 265 nm excites the pABA molecules, an electron from the ground singlet state (S_0) is transferred to the excited singlet state (S_1).The excited molecules undergo non-radiative intersystem crossing (ISC) from short lived (S_1) state to a long-lived triplet (T_1) state. G. Meijer *et.al* reported that the triplet state of pABA lies between 1.57 (12653cm^{-1}) and 3.00 eV (24177cm^{-1}) above the singlet ground state.[46] However, as the $^5D_4$ state of Tb^{3+}ion is 2.54 eV (20500 cm^{-1})[47] which lies in between the triplet state of pABA, energy is transferred from the higher triplet state to the low lying accepting levels of Tb^{3+}. This transferred energy from antenna (pABA) excites 4f electrons of Tb^{3+} to the higher energy levels. Radiative transitions from$^5D_4$-^7F_J (J = 4–6) of Tb^{3+} ions gives its typical three characteristic strong emission bands centred at 490 nm, 546 nm and 586 nm, among which the peak at 546 nm is the strongest one. Sensitised luminescence intensity increases with

increase in Tb^{3+} ion concentration in the LaF_3 nanoparticles (Figure S3, See ESI) which is quite understandable that with the increase of the concentration of the emitter entity, the emission is tend to increase accordingly. But at 10% Tb^{3+} concentration luminescence reduces due to concentration quenching which is a phenomenon where at higher concentration the emitted radiation from one moiety is absorbed by the another nearby moiety and leading to the over reduction of the final emitted radiation from the sample. In this present study, the optimum concentration of the Tb^{3+} ion is found to be 8 at %.

3.5.1 Variation on the photoluminescence properties with change of pH

As the pH of the aqueous solutions plays a vital role on the luminescence property of functionalised materials, pABA functionalised LaF_3:Tb^{3+} (8%) were analysed at different pH values. To each of 250 ml of aqueous solutions of different pH, 50 mg of surface functionalised LaF_3:Tb^{3+} (8%) particles were added and nicely dispersed.

All the samples were excited at 265 nm and variation in luminescence intensity of these samples were recorded in the wavelength range of 450-700 nm (Figure 4). In very strong acidic medium (pH = 1) luminescence gets switched off due to protonation of the amine group. The luminescence intensity again reappears at pH = 2 and shows maximum luminescence at pH = 3 due to the occurrence of the $–NH_2$ state of pABA as explained above. Luminescence intensities in the pH range of 4-7 are almost same as shown in Figure 4a. The integrated area of 546 nm peak also shows that maximum at pH = 3 (inset of Figure 4a). After pH = 7, a slight enhancement in the luminescence is observed till pH = 9. In the strong alkaline medium (pH = 10-13), luminescence reduces below the neutral medium luminescence (Figure 4b). Very low luminescence intensity in strongly acidic medium (pH = 1) and strongly alkaline medium (pH = 13) is experimentally supported by very low UV absorption intensities at that pH values (Figure S2, See ESI). Surface area to volume ratio ($4\pi r^2/4\pi r^3/3$) of these very small nanoparticles (~5 nm) is around10^7 cm^{-1}. Under this condition, a significant number of Tb^{3+} ions on the surface of the nanoparticles will form co-ordinate bond with the hydroxyl ion in strong alkaline medium. Excited states of Tb^{3+} ions are non-radiatively quenched by the -OH group vibrations.[48] Our research group has also previously reported that the luminescence of lanthanide ions are quenched by the presence of O-H group in the compound.[49,50] This nonradiative quenching as well as the low dispersibility of the nanoparticles in strong alkali explains the observed decrease in luminescence. Low dispersibility of the particles in alkaline medium arises due to the basic nature of the particles,

which is due to the presence of free $–NH_2$ group on the particle surface. Luminescence quenching in the alkaline medium (pH = 9-13) shows a linear relationship with pH of the medium. A plot of integrated area of the most intense peaks at 546 nm vs pH shows a straight line having negative slope and taking an intercept on y-axis (Inset of Figure 4b). This linear relationship can be used to detect pH of unknown alkaline medium. Overall, by studying the variation of the photoluminescence properties of the pABA sensitised $LaF_3:Tb^{3+}$ nanomaterials at different pH, these materials will have potential application in the detection of pH of an unknown solution.

3.5.2 Detection of nitro explosives

pABA surface functionalised $LaF_3:Tb^{3+}$ nanoparticles can detect highly electron deficient aromatic nitro compounds at very low concentrations . Equal volume of the dispersion of the pABA functionalised $LaF_3:Tb^{3+}$ nanoparticles and the aqueous solution of the nitro compounds were mixed and their photoluminescence properties were recorded at pH = 3. We conducted this experiment for some selected aromatic nitro compounds such as nitrobenzene (NB), o-nitrophenol (2-NP), o-nitrotoluene (2-NT), 2,4-dinitrotoluene (2,4-DNT), 2,6-dinitrotoluene (2,6-DNT), 2,4-dinitrophenol (2,4-DNP), picric acid (PA) and 2,4,6-trinitrotoluene (TNT) and some selected aliphatic nitro compounds such as nitromethane, 1,2,4-butanetriol nitrate (BTTN), octahydro-1,3,5,7-tetranitro-1,3,5,7-tetrazocine (HMX), and 1,3,3-Trinitroazetidine(TNAZ).

Figure 5 shows luminescence quenching of $LaF_3:Tb^{3+}$@pABA by picric acid and TNT. Quenching is even observed at very low concentrations of TNT (10 ppm or 50μM) and picric acid (2.25 ppm or 10μM). Figure 6 shows that NP, 2,4-DNP and 2,4-DNT can also quench the luminescence at very low concentrations (12.5μM). Figure S4 shows very sensitive detection of TNT at ppb level. At such low concentration the luminescence intensity change at $^5D_4$-$^7F_4$ is more clearly seen than for $^5D_4$-$^7F_5$ transition. The luminescence at 490 nm was used for Stern-Volmer plot. The surface functionalised nanomaterials were able to detect TNT up to 50 ppb.

Nature of the quenching can be understood from the respective plots of I_0/I *vs* concentrations [Q]. At low concentrations of the analyte, the quenching of luminescence by the acceptor molecules follow the classic Stern-Volmer relationship, $I_0/I = 1+k_Q[Q]$ where k_Q is the quenching constant, I is the intensity of fluorescence at the quencher concentration [Q], and I_0 is the fluorescence intensity in the absence of quencher.[51,52] Calculated values of

quenching constant (k_Q), obtained using above Stern-Volmer equation for TNT, PA, 2-NP, 2,4-DNT, 2,4-DNP are 12295, 5738, 1683, 3296, 2103M^{-1} respectively. Among the above analysed nitrocompounds, TNT has remarkably high quenching constant. At higher analyte concentrations, I_0/I *vs* [Q] plot show upward curvature. At these concentrations the fluorescence quenching follow $I_0/I = (1+k[Q])\ (1+k^{obsd}\tau_0[Q])$ equation.[53] A comparison of quenching efficiencies of the all the selected nitrocompounds at a particular concentration (0.1mM) is shown in the bar-graph of Figure 7. Quenching efficiencies (%) are calculated using the formula $(I_0 - I)/I_0 \times 100\%$, where I_0 is the maximum fluorescence intensity of the functionalised nanoparticles before exposure to the NPs, and I is after interaction with the nitrocompounds. It shows negligible quenching by aliphatic nitroexplosives except for RDX (explained below). Thus the nanoparticles are highly sensitive to the selected aromatic nitroexplosives.

The order of quenching is as follows;
2,4-DNT > 2-NP > 2,4-DNP > NB, TNT > PA > RDX > 2,6-DNT >> NT > TNAZ > HMX > NM, BTTN.

The observed fluorescence quenching can be explained by the donor-acceptor electron-transfer mechanism and energy transfer mechanism. The aromatic trinitro explosives have low-lying π*-type lowest unoccupied molecular orbital (LUMO) which is stabilised by the electron withdrawing -NO_2 group. Electron can transfer from the higher energy triplet state of pABA to the LUMO of the aromatic nitro analyte.[54,55] Thus energy transfer from pABA to Tb^{3+} decreases in presence of aromatic nitrocompounds and results in luminescence quenching. Now it is well established that analytes with more negative LUMO energy and consequently less negative reduction potential exhibit a larger driving force for electron transfer from particles to quenchers.[56,57] Energy of LUMO of most of the aliphatic nitroexplosives lies above that of pABA and hence no electron transfer as well as luminescence quenching is observed by the aliphatic nitro explosives (Figure S5, See ESI). To explain the above quenching efficiency sequence where the non-explosive or less explosives aromatic compounds like 2,4-DNT, 2-NP, 2,4-DNP having less number of electron withdrawing –NO_2 group show very much potent quenching ability, we need to consider the energy transfer mechanism in addition to electron transfer mechanism. The energy transfer mechanism is supported by non-linear nature of Stern-Volmer plot. A non-

linear Stern-Volmer equation indicates super amplified quenching.[58,59] Fluorophore to analyte energy transfer can occur if the fluorophore and analyte are close to each other and the absorption band of the analyte overlaps effectively with the emission band of the fluorophore.[60]

Figure 8 shows that emission spectra of pABA overlaps effectively with the UV absorption spectra of 2,4-DNT, 2-NP, 2,4-DNP and picric acid. This can explain high quenching performance of less explosive or non-explosive 2,4-DNT, 2-NP and 2,4-NP. In these cases in addition to electron transfer, energy transfer from pABA to analyte occurs as well. There is a very less overlap for 2,6-DNT, TNT and RDX. So the quenching mechanism for 2,6-DNT, TNT and RDX is mainly electron transfer mechanism. This observation can also explain very low quenching performance by 2,6-DNT and RDX. From the above analysis, we conclude that pABA sensitised $LaF_3:Tb^{3+}$ NPs can be potential materials for using as a sensor for the detection of highly explosive aromatic nitrocompounds.

3.5.3 Effect of laser irradiation

At a particular concentration of the nanoparticles and pH, the samples of varying concentrations of TNT and PA were irradiated with a ultraviolet (λ = 248 nm) KrF excimer laser (Lambda Physik-Germany) having a maximum average power of 40 watts (pulse energy = 150 mJ) and a pulse width of 20 ns to visualise the luminescence quenching by the explosive materials. Photographic images for the change in luminescence of pABA sensitised $LaF_3:Tb^{3+}$ NPs by the explosives at various concentrations has been shown in Figure 9. The concentration variations were done upto 60 ppm and 250 ppm for TNT and PA respectively. Even 20 ppm of TNT can quench the luminescence significantly where almost no fluorescence has been observed in presence of 60 ppm of TNT. This observation also supports the luminescence quenching pattern as shown in the Figure 5(b). Luminescence quenching by PA is very strong only at higher concentration, which is supported by Figure 5(a).

3.5.4 Lifetime measurements

Life-time of the nanoparticles was studied in presence and absence of the analytes (PA and TNT) and was recorded by fixing the excitation and emission wavelengths at 265 nm and 546 nm respectively as shown in Figure S6 (See ESI). Life time of the surface functionalised nanoparticles in absence of any analyte is 0.1177 ns. Life time values

decreases in presence of aromatic analytes. In presence of 18, 61.25 and 125 ppm picric acid life time values are 0.1158, 0.0883, and 0.0806 ns respectively. Life time values for 10, 20 and 60 ppm TNT are 0.0790, 0.0889, and 0.0785 ns respectively. In case of sensitised photoluminescence it is well established that life time of the sensitizer gradually decreases with the increase in the activator concentration.[61,62] In the present case life time of Tb^{3+} ion reduces with increase in the aromatic analyte concentration due to transfer of energy from the excited pABA molecule to the analyte molecules.

4. CONCLUSION

In summary, a novel approach for the detection of highly explosive aromatic nitro compounds and determination of pH of a solution utilizing the pABA sensitised terbium (Tb^{3+}) doped spherical LaF_3 nanoparticles has been reported. The as-prepared pABA functionalised nanoparticles show remarkable (>100 times) enhancement in the luminescence intensity as compared to the as-prepared non-functionalised compounds due to effective energy transfer from *p*-aminobenzoic acid to Tb^{3+}ion. This work establishes pABA as a very good sensitizer for Tb^{3+} ion. This functionalised nanomaterials show great influence of pH on their luminescence properties and can be used for the determination of pH of unknown solutions. We used this functionalised particles to determine the concentration of nitro compounds in aqueous medium. Luminescence intensity decreases exponentially with increase in the nitro compounds concentrations due to quenching of the excited states of the *p*-aminobenzoic acid by nitro compounds. The detection at ppm level is quite easily achieved for all the compounds but for TNT the nanoparticles show very high sensitivity up to 50 ppb level. The novel technique of utilising the Tb^{3+} doped NPs sensitised by pABA have potential application in the detection of explosives.

ACKNOWLEDGEMENTS

One of the authors (D Ghosh) would like to thank Council of Scientific and Industrial Research (CSIR) for research fellowship.

Notes

The authors declare no competing financial interest.

†Electronic Supporting Information (ESI) available:

Histogram showing the particle size distribution (DLS measurement) of LaF_3:Tb^{3+}@pABA nanoparticles. Absorption spectra of of LaF_3:Tb^{3+}@pABA nanoparticles at different pH, Emission spectra of LaF_3:Tb^{3+}@pABA nanoparticles at different concentration of Tb^{3+} ions, Emission spectra of LaF_3:Tb^{3+}@pABA nanoparticles at λ_{ex} = 265 nm with the change in concentration of TNT (ppb level). Inset shows their respective Stern-Volmer plots. Energy level diagramme of all the selected nitro compounds along with the decay profile for LaF_3:Tb^{3+}@pABA nanoparticles at varying concentration of (a) PA and (b) TNT.

REFERENCES

1. Y. Salinas, R. Martinez-Manez, M. D. Marcos, F. Sancenon, A. M. Castero, M. Parra and S. Gil, *Chem. Soc. Rev*., 2012, **41**, 1261.
2. Y. Yinon, *Forensic and Environmental Detection of Explosives*, John Wiley & Sons, Chichester, 1999.
3. W. C. Trogler, *Electronic Noses & Sensors for the Detection of Explosives* (Eds.: J. W. Gardner, J. Yinon), Kluwer Academic Publishers, Dordrecht, The Netherlands, 2004.
4. M. E. Germain and M. J. Knapp, *Chem. Soc. Rev*., 2009, **38**, 2543.
5. T. L. Andrew and T. M. Swager, *J. Am. Chem. Soc.*, 2007, **129**, 7254.
6. S. J. Toal and W. C. Trogler, *J. Mater. Chem*., 2006, **16**, 2871.
7. *Toxicological Profile for 2,4,6-Trinitrotoluene, Agency for Toxic Substances and Disease Registry*, US Department of Health and Human Services, Atlanta, GA, 1995.
8. S. Letzel, T. Goen, M. Bader, J. Angerer and T. Kraus, *Occup. Environ. Med.*, 2003, **60**, 483.
9. A. Jarvi, E. Leinonen, M. Thompson and K. Valkonen, *Designing Modern Walk-through Metal Detectors, Access Security Screening: Challenges and Solutions*, ASTM STP 1127 TP Tsacoumis Ed, American Society for Testing of Materials, Philadelphia 1992, **21**.
10. I. Gazit and J. Terkel, *Appl. Anim. Behav. Sci*., 2003, **81**, 149.
11. K. Wells and D. A. Bradley, *Applied Radiation and Isotopes*., 2012, **70**, 1729.
12. E. T. H. Clifford, J. E. McFee, H. Ing, H. R. Andrews, D. Tennant, E. Harper and A. A. Faust, *Nuclear Instrum. Methods Phys. Res. A.,* 2007, **579**, 418.

13. M. S. Meaney and V. L. McGuffin, *Anal. Bioanal. Chem*., 2008, **391**, 2557.
14. J. H. Lee, J. Jaworski and J. H. Jung, *Nanoscale.,* 2013, **5**, 8533.
15. K. K. Kartha, S. S. Babu, S. Srinivasan and A. Ajayaghosh, *J. Am. Chem. Soc*., 2012, **134**, 4834.
16. M. E. Germain and M. J. Knapp, *Chem. Soc. Rev*., 2009, **38**, 2543.
17. D. A. Olley, E. J. Wren, G. Vamvounis, M. J. Fernee, X. Wang, P. L. Burn, P. Meredith and P. E. Shaw, *Chem. Mater*., 2011, **23**, 789.
18. E. S. Snow, F. K. Perkins, E. J. Houser, S. C. Badescu and T. L. Reinecke, *Science.* 2005, **307**, 1942.
19. S. S. Nagarkar, B. Joarder, A. K. Chaudhari, S. Mukherjee and S. K. Ghosh, *Angew. Chem. Int. Ed*., 2013, **125**, 2953.
20. G. L. Liu, Y. J. Qin, L. Jing, G. Y. Wei and H. Li, *Chem. Commun*., 2013, **49**, 1699.
21. Y. Liu, D. Tu, H. Zhu and X. Chen, *Chem. Soc. Rev*., 2013, **42**, 6924.
22. R. J. Crutchley, *Coordination Chem. Rev*., 2014, **273-274**, 1.
23. P. Yang, S. Gaib and J. Lin, *Chem. Soc. Rev.,* 2012, **41**, 3679.
24. S. Gai, C. Li, P. Yang, and J. Lin, *Chem. Rev.,* 2014, **114**, 2343.
25. H. Tsukube and S. Shinoda, *Chem. Rev.,* 2002, **102**, 2389.
26. C. Lescop, D. Luneau, G. Bussiere, M. Triest and C. Reber, *Inorg. Chem.,* 2000, **39**, 3740.
27. J. Zhang, C. M. Shade, D. A. Chengelis and S. Petoud, *J. Am. Chem. Soc.,* 2007, **129**, 14834.
28. M. N. Luwang, R. S. Ningthoujam, S. K. Srivastava and R. K. Vatsa, *J. Mater. Chem*., 2011, **21**, 5326.
29. A. J. Keynon, *Progress in Quantum Electronics.,* 2002, **26**, 225.
30. S. Gai, P. Yang, X. Li, C. Li, D. Wang, Y. Daib, and J. Lin *J. Mater. Chem.,* 2011, **21**, 14610.
31. C. Li and J. Lin, *J. Mater. Chem.,* 2010, **20**, 6831.
32. A. M. Cross, P. S. May, F. C. J. M. Veggel and M. T. Berry, *J. Phys. Chem. C.,* 2010, **114**, 14740.
33. J. Wang, Z. Wang, X. Li, S. Wang, H. Mao and Z. Li, *Applied Surface Science.,* 2011, **257**, 7145.
34. S. Li, X. Zhang, Z. Hou, Z. Cheng, P. Maa and J. Lin, *Nanoscale.,* 2012, **4**, 5619.
35. Y. Ma, S. Huang and L. Wang, *Talanta.,* 2013, **116**, 535.

36. L. Honga, Q. Mei, L. Yang, C. Zhang, R. Liu, M. Han, R. Zhanga and Z. Zhang, *Analytica Chimica Acta.,* 2013, **802**, 89.
37. C. Dong, M. Raudsepp and F. C. J. M. Veggel, *J. Phys. Chem. C.,* 2009, **113***,* 472.
38. M. Yao, A. G. Joly and W. Chen, *J. Phys. Chem. C.,* 2010, **114***,* 826.
39. K. Sawada, K. Abdel-Aal, K. Tana, and K. Satoh, *Dalton Trans.,* 2005, **20**, 3291.
40. W. C. Wu, C. C. Chuang and J. L. Lin, *J. Phys. Chem. B.,* 2000, **104***,* 8719.
41. J. Ma, P. Huang, M. He, L. Pan, Z. Zhou, L. Feng, G. Gao and D. Cui, *J. Phys. Chem. B.,* 2012, **116**, 14062.
42. C. J. Kern, T. Antoshkiw and R. Maiese, *Anal. Chem*., 1948, **20**, 919.
43. I. M. Klotz and D. M. Gruen, *J. Am. Chem. Soc.,* 1945, **67**, 843.
44. W. D. Kumler and L. A. Strait, *J. Am. Chem. Soc.,* 1943, **65**, 2349.
45. K. Venkateswaran, J. M. Stadlbauer, Z. Wu, H. A. Gillis and D. C. Walker, *J. Phys. Chem.,* 1996, **100***,* 3569.
46. G. Meijer, M. S. Vries, H. E. Hunziker, H. R. Wendt, *J. Chern. Phys*., 1990, **92**, 7625.
47. Y. J. Li and B. Yan, *Inorg. Chem*., 2009, **48**, 8276.
48. S. Nigam, V. Sudarsan and R. K. Vatsa, *J. Phys. Chem. C.,* 2009, **113***,* 8750.
49. M. N. Luwang, R. S. Ningthoujam, Jagannath, S. K. Srivastava and R. K. Vatsa, *J. Am. Chem. Soc.,* 2010, **132**, 2759.
50. M. N. Luwang, R. S. Ningthoujam, S. K. Srivastava and R. K. Vatsa, *J. Am. Chem. Soc.,* 2011, **133**, 2998.
51. W. Wei, X. Huang, K. Chen, Y. Tao and X. Tang, *RSC Advances.,* 2012, **2**, 3765.
52. J. Wang, J. Mei, W. Yuan, P. Lu, A. Qin, J. Sun, Y. Mac and B. Z. Tang, *J. Mater. Chem.,* 2011, **21**, 4056.
53. J. Keizer, *J. Am. Chem. Soc.,* 1983, **105***,* 1494.
54. S. Pramanik, C. Zheng, X. Zhang, T. J. Emge and J. Li, *J. Am. Chem. Soc.,* 2011, **133**, 4153.
55. T. Pazhanivel, D. Nataraj, V. P. Devarajan, V. Mageshwari, K. Senthiland, D. Soundararajan, *Anal. Methods.,* 2013, **5**, 910.
56. W. Chen, N. B. Zuckerman, J. P. Konopelski and S. Chen, *Anal. Chem.,* 2010, **82**, 461.
57. J. Li, C. E. Kendig, E. E. Nesterov, *J. Am. Chem. Soc*., 2007, **129**, 15911.
58. J. Liu, Y. Zhong, P. Lu, Y. Hong, J. W. Y. Lam, M. Faisal, Y. Yu, K. S. Wong and B. Z. Tang, *Polym. Chem.,* 2010, **1**, 426.

59. D. Zhao and T. M. Swager, *Macromolecules.,* 2005, **38**, 9377.
60. S. S. Nagarkar, B. Joarder, A. K. Chaudhari, S. Mukherjee and S. K. Ghosh, *Angew. Chem. Int. Ed.,* 2013, **52**, 2881.
61. P. Banerjee, S. Pramanik, A. Sarkar and S. C. Bhattacharya, *J. Phys. Chem. B.,* 2009, **113***,* 11429.
62. S. Chall, S. S. Mati, S. Rakshit and S. C. Bhattacharya, *J. Phys. Chem. C.,* 2013, **117**, 25146.

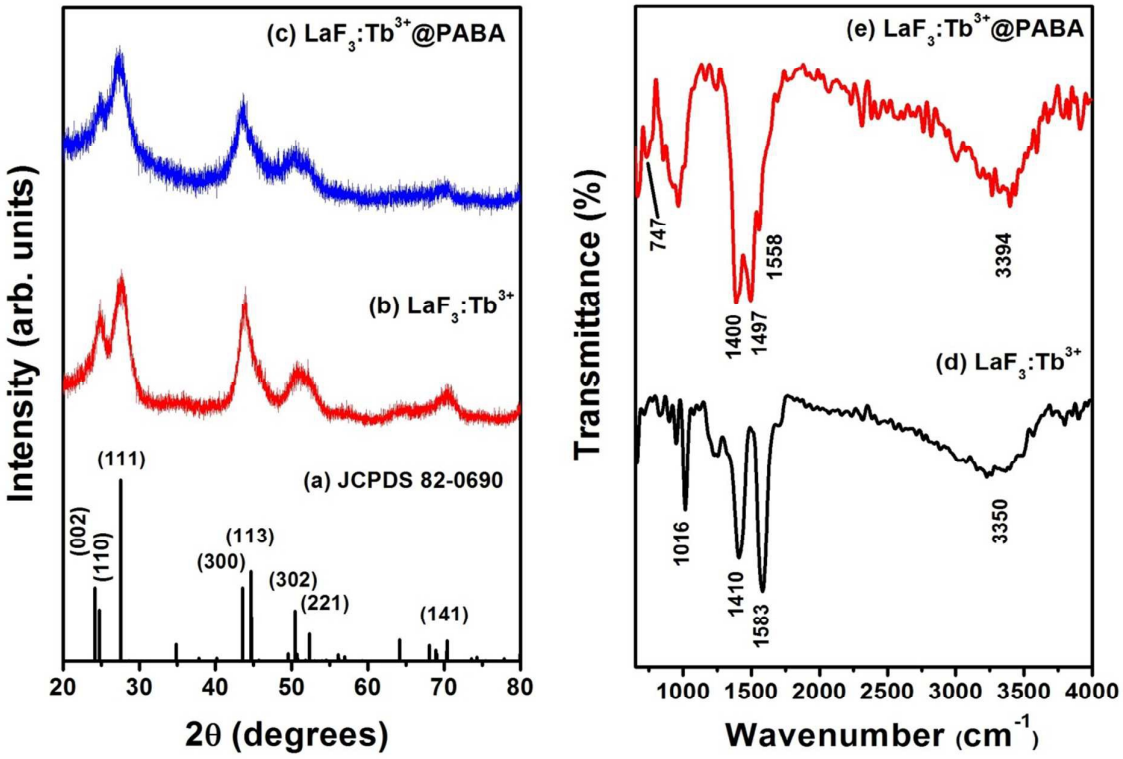

Figure 1: XRD and IR spectra of $LaF_3:Tb^{3+}$ nanoparticles with and without pABA along with the JCPDS Card No. 82-0690.

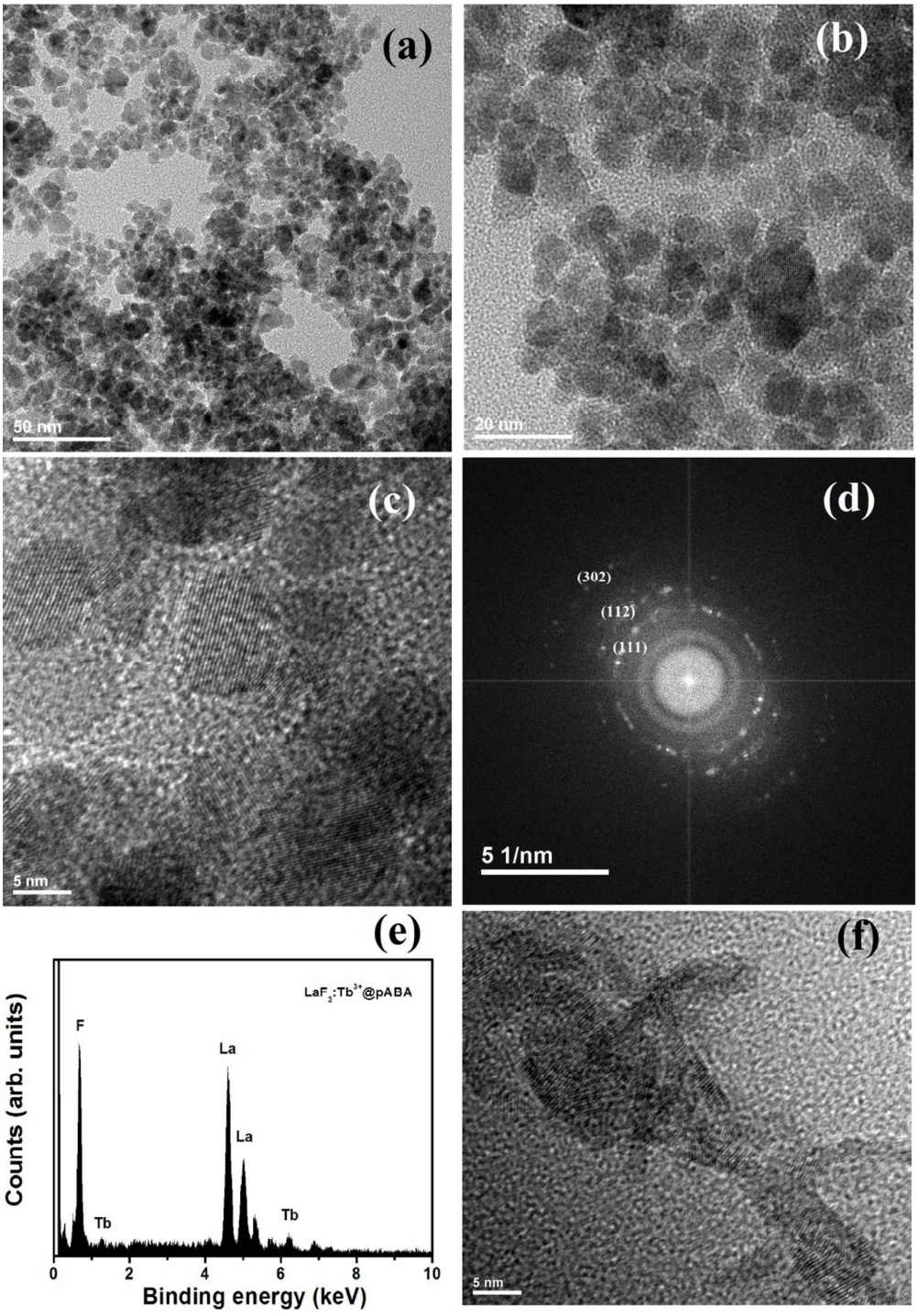

Figure 2: Images showing the morphology of $LaF_3:Tb^{3+}$@pABA nanoparticles (a-c) along with (d) its SAED and (e) its EDAX spectra. Rod shape morphology of higher dopant concentration is also shown (f).

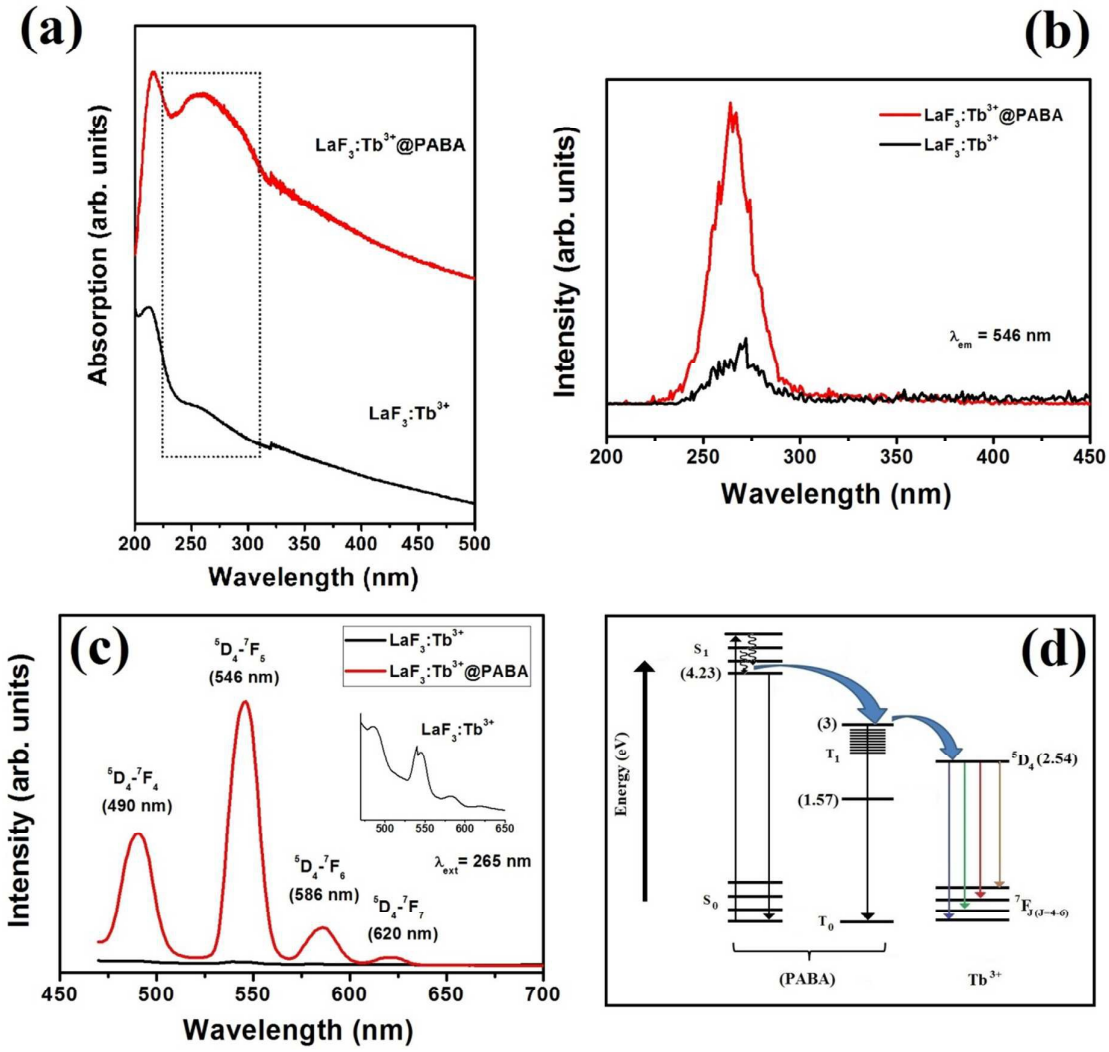

.

Figure 3: (a) Absorption, (b) excitation and (c) emission spectra of $LaF_3:Tb^{3+}$ with and without pABA along with (d) schematic diagramme for the energy transfer in $LaF_3:Tb^{3+}$@pABA nanoparticles. Excitation and emission wavelength are fixed at 265 and 546 nm, resp.

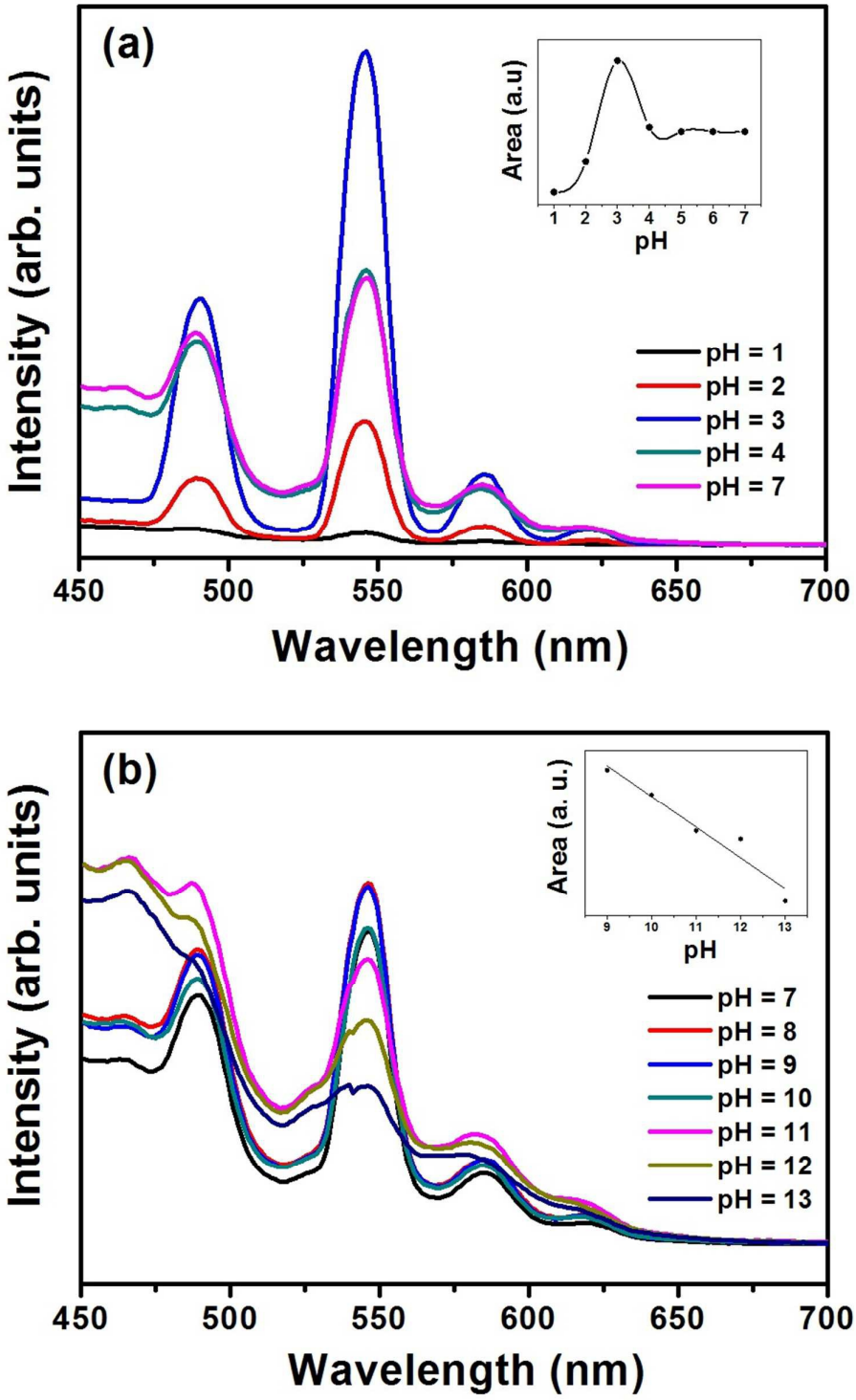

Figure 4: Effect of pH on the emission spectra $LaF_3:Tb^{3+}$@pABA nanoparticles at λ_{ex} = 265 nm. Inset shows the integrated area under the curve for 546 nm peak.

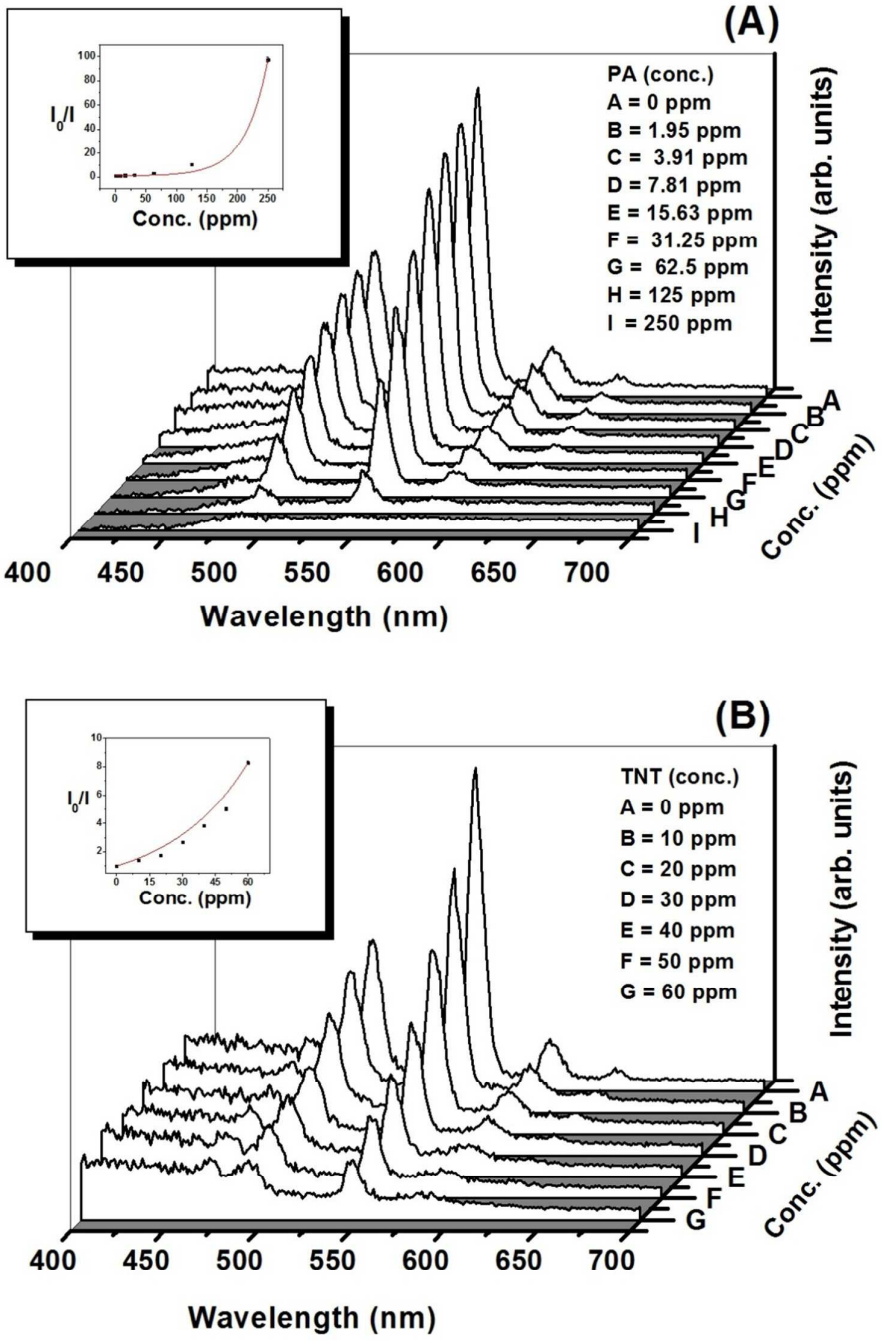

Figure 5: Emission spectra of $LaF_3:Tb^{3+}$@pABA nanoparticles at λ_{ex} = 265 nm with the change in concentration of (a) PA and (b) TNT. Inset shows their respective Stern-Volmer plots.

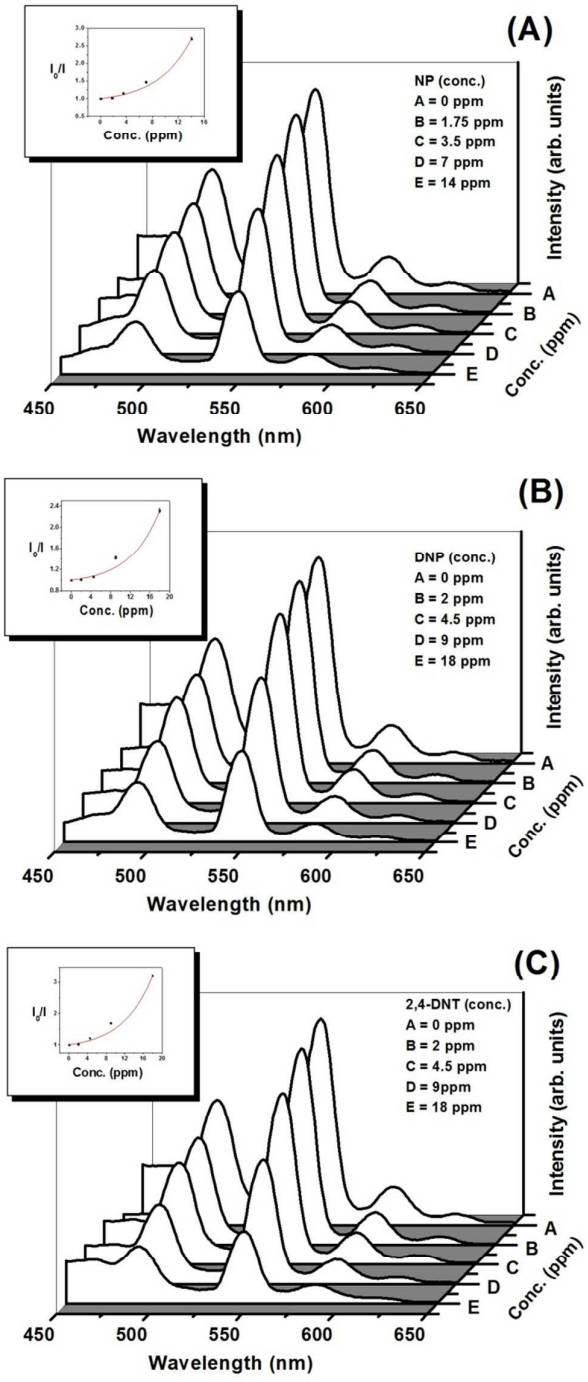

Figure 6: Emission spectra of $LaF_3:Tb^{3+}$@pABA nanoparticles at λ_{ex} = 265 nm with the change in concentration of (a) NP, (b) DNP and (c) DNT. Inset shows their respective Stern-Volmer plots.

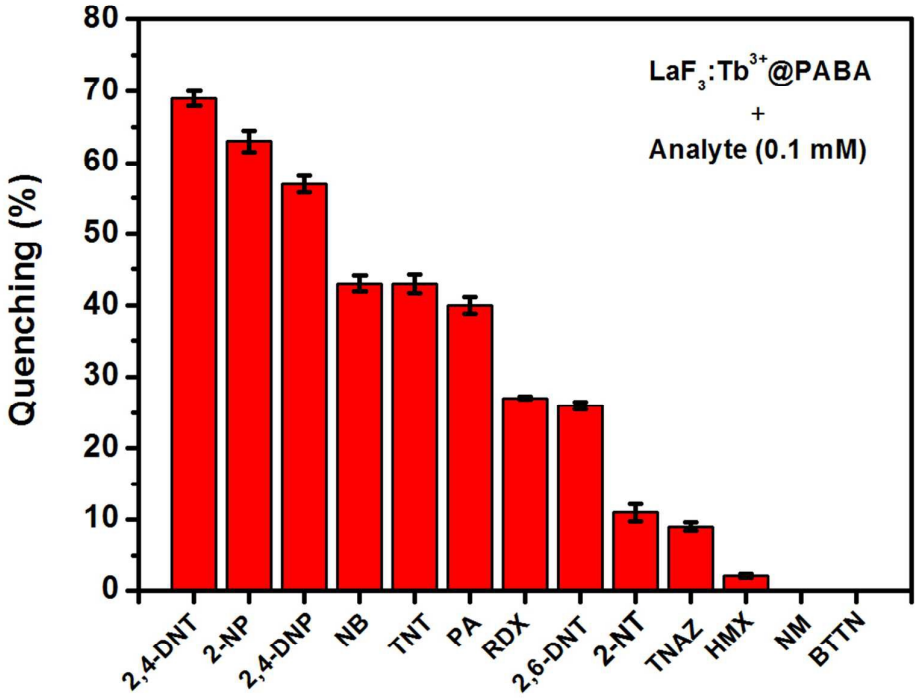

Figure 7: Bar graph showing the quenching efficiencies (%) for all the analysed analyte at their fixed concentration of 0.1 mM.

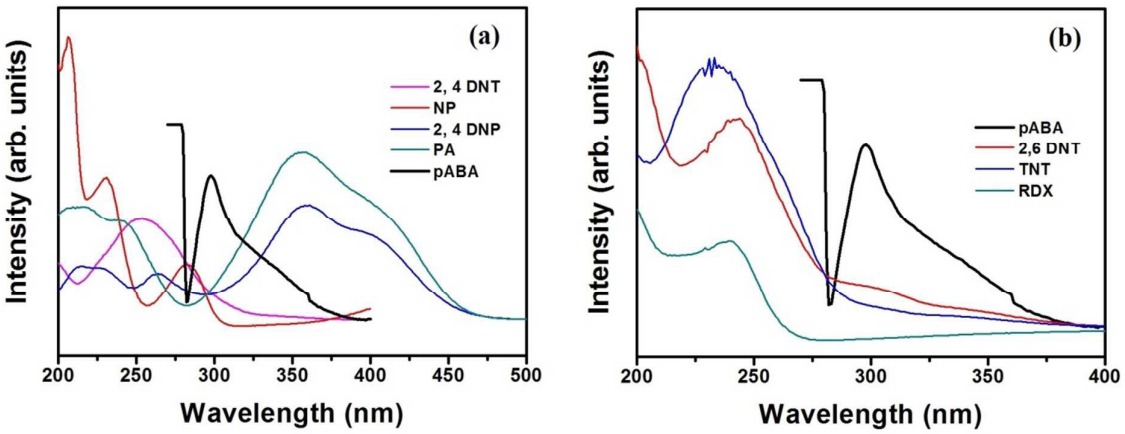

Figure 8: UV absorption spectra of pABA along with (a) NP, 2,4-DNP, PA, DNT and (b) 2,6-DNT, TNT, RDX.

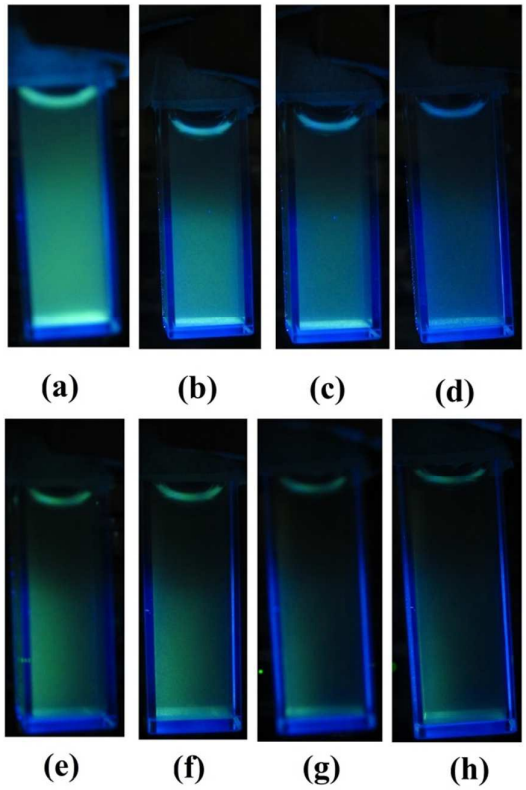

Figure 9: Photographic images for the variation in luminescence of $LaF_3:Tb^{3+}$ NPs on laser irradiation (248 nm) in presence of (a) 0 ppm analyte (b) 20 ppm TNT (c) 40 ppm TNT (d) 60 ppm TNT (e) 31 ppm PA (f) 62 ppm PA (g) 125 ppm PA and (h) 250 ppm PA.

Table 1: Crystallite size, Lattice parameter, Unit cell volume and FWHM of pABA functionalised and non-functionalised $LaF_3:Tb^{3+}$ NPs.

Sl. no	Sample	Crystallite size (nm)	Lattice parameter		Unit cell volume ($Å^3$)	FWHM (111)
			a=b	c		
1	$LaF_3:Tb^{3+}$ (2%)	5.52	7.19	7.43	332.90	2.70
2	$LaF_3:Tb^{3+}$ (4%)	5.90	7.17	7.44	331.99	2.50
3	$LaF_3:Tb^{3+}$ (6%)	5.74	7.17	7.50	334.10	2.61
4	$LaF_3:Tb^{3+}$ (8%)	5.59	7.17	7.42	330.95	2.71
5	$LaF_3:Tb^{3+}$ (10%)	6.29	7.16	7.31	325.23	2.49
6	$LaF_3:Tb^{3+}$ (2%)@PABA	4.50	7.19	7.43	340.67	3.12
7	$LaF_3:Tb^{3+}$ (4%)@PABA	5.28	7.17	7.44	336.10	2.70
8	$LaF_3:Tb^{3+}$ (6%)@PABA	5.08	7.17	7.50	341.27	2.93
9	$LaF_3:Tb^{3+}$ (8%)@PABA	4.57	7.17	7.42	338.62	3.02
10	$LaF_3:Tb^{3+}$ (10%)@PABA	5.53	7.16	7.31	332.71	3.14